

Geophysical Research Letters®



RESEARCH LETTER

10.1029/2024GL109353

Sprite Durations Measured With a Neuromorphic Sensor

B. Smith¹ , M. G. McHarg², C. L. da Silva¹ , R. G. Sonnenfeld¹ , J. Koile³, A. F. R. Leal¹ , and I. R. Jones⁴ 

Key Points:

- Fast speeds and low data rates potentially make neuromorphic cameras ideal for observation of sprites and lightning
- Neuromorphic sensors can measure sprite durations in good agreement with high frame rate cameras
- Sprites are very dim making it challenging for the neuromorphic sensor to resolve their internal spatiotemporal dynamics

Supporting Information:

Supporting Information may be found in the online version of this article.

Correspondence to:

C. L. da Silva,
caitano.dasilva@nmt.edu

Citation:

Smith, B., McHarg, M. G., da Silva, C. L., Sonnenfeld, R. G., Koile, J., Leal, A. F. R., & Jones, I. R. (2024). Sprite durations measured with a neuromorphic sensor. *Geophysical Research Letters*, 51, e2024GL109353. <https://doi.org/10.1029/2024GL109353>

Received 18 MAR 2024
Accepted 20 MAY 2024

¹Department of Physics & Langmuir Lab, New Mexico Tech, Socorro, NM, USA, ²Department of Physics, U.S. Air Force Academy, Colorado Springs, CO, USA, ³Department of Physics & Astronomy, Space Science Center (EOS), The University of New Hampshire, Durham, NH, USA, ⁴International Centre for Neuromorphic Systems, Western Sydney University, Werrington, NSW, Australia

Abstract Neuromorphic sensors have inherently-fast speeds and low data rates, which potentially make them ideal for the observation of transient sources, such as lightning and sprites. Particularly, for remote observations. In this article, we report the first observations of sprites from the ground with a neuromorphic sensor. These observations are accompanied by measurements with established instruments such as low-light level and high-frame rate cameras. We determine that neuromorphic sensors can capture sprites and determine their duration to an accuracy of roughly 6 ms. Average sprite durations were found to be 55 ms within our data set. We have also ascertained that sprites may be too dim for the neuromorphic sensors to resolve the internal spatiotemporal dynamics, at least without the aid of intensifiers.

Plain Language Summary Neuromorphic sensors are a relatively new tool with great potential for imaging transient sources. Neuromorphic sensors track light changes in individual pixels and only store information when the light intensity surpasses a pre-set threshold, a design choice made with the intent of mimicking how the human eye works. Sprites and lightning are fast, transient light sources and, thus, are an ideal target to test this new technology. In this work, we report the first observations of sprites from the ground with a neuromorphic sensor, and compare these observations with recordings made with an established and well-understood instrument: an intensified high-speed camera. Our results show that there is a lot of promise in using this new technology for observation of sprites and lightning, particularly for autonomous, long-duration observations. We conclude by speculating that the use of neuromorphic sensors in atmospheric sciences will grow substantially in the coming years. They will find many uses in autonomous optical instruments, such as employed for monitoring the aurora, atmospheric gravity waves, and bolide/fireball detection.

1. Introduction

Sprites are a type of transient luminous event which occur near the top of the mesosphere at about 80 km altitude in response to the electric field generated by lightning flashes in underlying thunderstorms (Boccippio et al., 1995; da Silva & São Sabbas, 2013; Luque & Ebert, 2009; Pasko, 2010; Pasko et al., 1997). Despite a wide range of amateur and citizen scientist observational efforts, campaigns to study the fundamental physics of sprites and their impacts in the upper atmosphere are still mostly done by research teams aided by expensive equipment (e.g., high frame rate cameras, radio antennas). One such example is the investigation on sprite durations. The energy dissipated by sprites in the mesosphere via Joule heating can be approximated according to the following equation:

$$\text{Energy dissipated} = \int RI^2 dt \approx \bar{R}\bar{I}^2 \times \text{duration}, \quad (1)$$

where R is the total resistance dependent on the conductivity and volume occupied by sprite streamers, and I is the electrical current traversing the sprite body vertically, which can be probed via radio remote sensing (e.g., Contreras-Vidal et al., 2021). Equation 1 makes the case that sprite durations can provide a direct measure of the energetic impacts of sprites in the mesosphere. This is true under the assumption that average \bar{R} and \bar{I} values do not change substantially across different events. At the very least, sprite durations are an important parameter to estimate total energy deposition. Besides radio-frequency remote sensing, infrasonic emissions can also reveal important information about currents within sprites (da Silva & Pasko, 2014). Another way of looking into the importance of sprite durations is to appreciate that the optical lifetime is indicative of the chemical lifetime of active

© 2024. The Author(s).

This is an open access article under the terms of the [Creative Commons Attribution-NonCommercial-NoDerivs License](https://creativecommons.org/licenses/by/4.0/), which permits use and distribution in any medium, provided the original work is properly cited, the use is non-commercial and no modifications or adaptations are made.

species introduced by sprites in the mesosphere (Gordillo-Vazquez, 2008; Sentman & Stenbaek-Nielsen, 2009; Sentman et al., 2003, 2008). Sentman et al. (2003) estimated the total energy deposition by a single sprite to be of the order of 1 MJ.

Estimates on sprite durations have mostly been done using Watec low-light level cameras, which operate at 30 frames per second (FPS) and have a maximum temporal resolution of 17 ms after the video is deinterlaced. Anecdotally, users of Watec cameras report sprite durations ranging from one (17 ms) to several frames (several tens of ms). The first estimates of sprite duration through video data were made by Rairden and Mende (1995) and since then there have been a few other investigations (Bór, 2013; Hardman et al., 2000; Montanyà et al., 2010). These authors placed the average sprite duration between 30 and 80 ms, with wide variation between events. Bór (2013) reports that long optical lifetimes of up to 160 ms can be observed when long-lasting optical features, such as spots, tendrils, puffs, or glows are present. We note that these duration figures contrast heavily with estimates from photometric measurements. Narrowband photometry, particularly near the blue portion of the visible spectrum, places sprite durations between 1 and a few ms (Armstrong et al., 2000; McHarg et al., 2002; Winckler et al., 1996).

A lot has been learned from high-speed (i.e., high-frame rate) observations of sprites, including: that sprites are most often initiated by downward streamers (columniform), which sometimes are followed by upward ones (carrots), that the speed of individual streamers is of the order of 10^7 m/s, that streamer heads grow exponentially in size and brightness until they branch, that streamer speed is proportional to its diameter, and that sprite streamers are most-favorably initiated from electron density inhomogeneities in the lower ionosphere (Qin et al., 2012, 2013, 2014; Stenbaek-Nielsen et al., 2013). However, the higher temporal resolution associated with high speed cameras comes at a cost. The two key drawbacks are: (a) these cameras are expensive preventing their widespread use and (b) high frame rates are accompanied by high data volumes. The latter fact means that these cameras are operated for only a fraction of the sprite duration, and always capture just a fraction of the sprites over a certain storm.

A new technology has surged with the potential of bridging the gap between the two observation regimes. Developed in the late 2000s, neuromorphic or event-based cameras/sensors are made to uniquely replicate the design of the human eye. Each pixel of the sensor operates independently and only reports changes in brightness which surpass a preset threshold, greatly reducing the required data rate by eliminating redundant information. These systems also carry the benefit of a higher dynamic range and a higher maximum “equivalent frame rate” than cameras of comparable cost (Holesovsky et al., 2021; McReynolds et al., 2023; Scheerlinck, 2021). These proposed higher speeds and significantly lower data rates in principle have a lot of potential for sprite observations.

Figure 1 briefly explains the process to obtain an image from a neuromorphic sensor. This is explained using one of the sprites from our data set, which is shown in Figure 1a, as detected by a 30-FPS, low-light level Watec camera. As schematically shown in Figure 1b, each pixel in a neuromorphic sensor captures events independently, generating an On or Off signal when a respective threshold is reached. If a pixel does not meet either threshold it does not give any signal, thus greatly cutting down the amount of data produced and allowing for much longer recordings than traditional video formats. The output data array includes a timestamp, pixel location (x, y), and polarity (On/Off) for each event. When this array is plotted to show event rates, such as in Figure 1c, spikes in the plot emerge, clearly demarcating the occurrence of sprites. Ten sprites were recorded during the 17-min interval shown. By overlaying all of the On events from a brief excerpt around a spike, a plot like Figure 1b can be generated, reconstructing what is seen by a conventional frame camera.

The inherently-fast nature of neuromorphic sensors combined with their low data rate make them ideal for the observation of fast transient sources such as sprites and lightning, particularly for remotely-operated, long-duration observations. These characteristics of neuromorphic sensors have inspired the development of three missions to observe lightning and sprites from the International Space Station (ISS) (Balthazor et al., 2023; Chanrion et al., 2023; McHarg et al., 2022). In this work, we report the first ground-based observations of sprites with a neuromorphic sensor, and compare them to conventional frame-based cameras. We show that there is a lot of promise in using this new technology, for instance for probing sprite durations. However, there are also fundamental observational limitations that arise from the fact that sprites are inherently-dim sources.

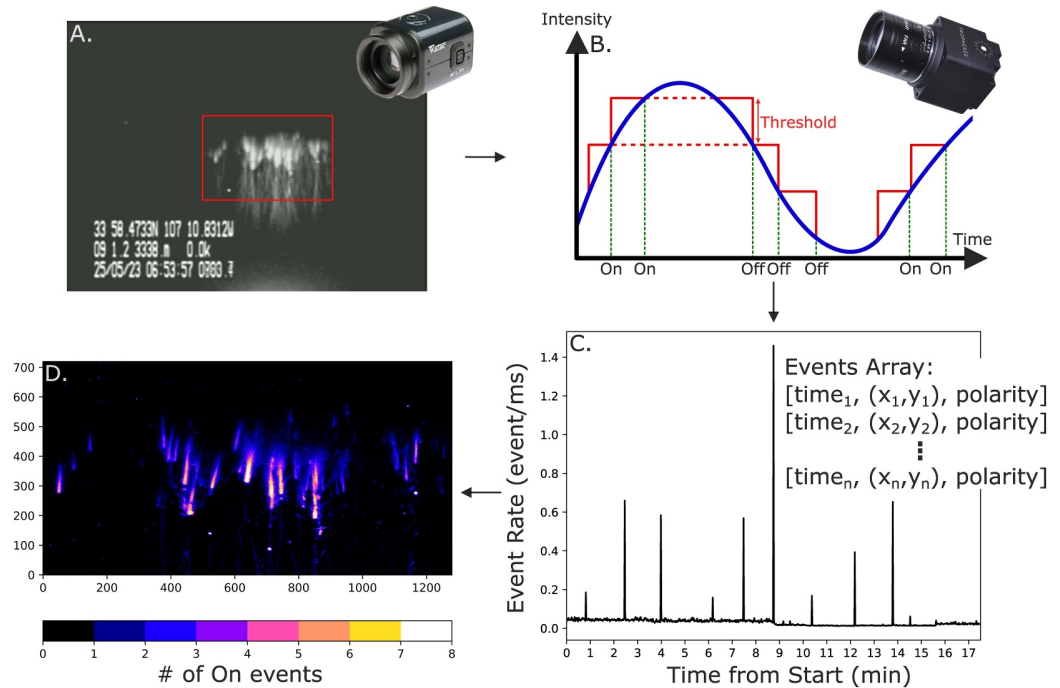


Figure 1. (a) A sprite, as observed with a Watec camera. (b) Schematic of logarithmic light intensity tracked by an individual pixel of a neuromorphic sensor, illustrating the On and Off events when the signal surpasses a preset threshold. (c) Event rate for a 17-min record of the neuromorphic sensor. Sprites naturally surge as spikes in the event rate. (d) Integrated image showing the cumulative number of On events in each pixel over a 20 ms period. Panel (a) shows the field of view of the neuromorphic camera with a red rectangle. Panel (b) is adapted from Brandli et al. (2014, Figure 2).

2. Data and Methods

On the night of 25 May 2023 we recorded several sprites from the Langmuir Laboratory for Atmospheric Research, located in central New Mexico, a site which has been extensively used for sprite research (Contreras-Vidal et al., 2021; Hager et al., 2012; Kanmae et al., 2007, 2012; Stenbaek-Nielsen et al., 2007, 2010). The sprite-parent storm took place in west Texas, approximately 500 km from the observation site. Among the recorded events, there are 9 sprites which were simultaneously captured by three different cameras:

- Generation 4 Prophesee EVK4 HD (hereafter referred to as the neuromorphic sensor). The camera was coupled with a 50-mm lens, resulting in a 7.1° field of view (FOV) in the horizontal direction. Typical data rate = 60 KB/s;
- Phantom v2640 operating at 34,000–60,000 FPS and coupled with a Video Scope VS4-1845HS intensifier (hereafter the Phantom camera). The camera was operated with a 300-mm f4 lens, resulting in a 2.4° FOV. This camera was operated on trigger mode, while the other two recorded continuously. Data rate = 16 GB/s;
- Watec WAT-902H2 (unintensified) low-light level camera operating at 30 FPS (hereafter the Watec camera), with a 25-mm lens, and 14° FOV. Data rate = 7 MB/s.

In this work, we shall compare the neuromorphic sensor to the widely-used Phantom and Watec cameras. Each pixel in a neuromorphic sensor independently detects changes in the logarithmic light intensity (see e.g., Figure 1b), in contrast to traditional frame-based cameras, which capture the entire frame at set intervals. Thus, the time interval between two events, $\text{time}_n - \text{time}_{n-1}$, can dynamically vary in the event stream data, being as short as 0 or 1 μs , or as large as the entire record. This results in a system which doesn't capture any superfluous data and has better time resolution than cameras of comparable price. The stream of data that is generated can be post-processed in various ways for different applications. The neuromorphic sensor images in this article have been constructed either to show the cumulative number of On events in each pixel (e.g., Figure 1c), or the time at which a pixel detects its first On event. These two methods are able to visualize the sprite's brightness and time dynamics, respectively. Furthermore, as discussed in the Results section, sprite "light curves" can be obtained by

creating bins with 4–8 ms durations and counting the number of On events within each period. A justification for the bin widths is provided later in the Results section. The light curves generated in this fashion were compared to those constructed from the Phantom camera, which was done by integrating the luminosity of all pixels in each frame (as was done in Contreras-Vidal et al. (2021) and Hager et al. (2012)). The Phantom imagery and light curves served as ground truth to compare the neuromorphic sensor to.

Sprites often have an apparent magnitude of -4 , comparable to the brightest stars in the sky (Stenbaek-Nielsen et al., 2013). Individual streamer heads can appear even brighter, with magnitudes of -6 (Stenbaek-Nielsen et al., 2007). These values are comparable to Venus' brightness, which is -4.6 in the stellar apparent magnitude logarithmic scale widely used in astronomy (Fraknoi et al., 2018, Chapter 17). Nonetheless, sprites and other astronomical objects are quite faint in comparison to typical applications of high-speed cameras, such as explosions, rocket launches, ballistics, etc., or just simply in comparison to video recordings in a well-lit environment ($\gtrsim 1$ klx, where $1 \text{ lx} = 1 \text{ lumen per square meter}$). In a similar fashion to high-speed cameras, in dim observational conditions neuromorphic sensors begin to face physical limitations due to decreased photocurrent on the receptor. As discussed by Hu et al. (2021) and McReynolds et al. (2023), an individual pixel in a neuromorphic sensor is in great part an analog circuit, with its bandwidth proportional to the photocurrent, that is, proportional to the light incident upon the sensor. For dim sources, the bandwidth may be substantially reduced to a point where the photoreceptor can no longer follow the fluctuations in the source luminosity. McReynolds et al. (2023, Figure 1) also discuss that the amplifier portion of the analog circuit closes after each event is recorded to allow the comparator to make a decision whether the new event meets a threshold and should be stored. This introduces dead time, referred to as the refractory period, which may vary between $1 \mu\text{s}$ to ~ 10 ms, depending on the camera settings. The generation 4 Prophesee camera allows the user to change a number of “biases,” which determine key sensor properties, including: independent On and Off thresholds (`bias_diff_on` and `bias_diff_off`), low-pass filter corner frequency (`bias_fo`), and refractory period (`bias_refr`). The caveat is that these biases are adjusted in a scale that does not have physical units and must, therefore, be optimized in an empirical manner (and this is what we did for the observations reported here). The biases used during the 25 May 2023 observations are listed, alongside the entire data set, in the data repository (Smith et al., 2024). Bearing in mind all the potential advantages and shortcomings of this new technology, in this article, we explore to what extent an unintensified neuromorphic sensor can resolve the temporal dynamics within sprites.

3. Results

Figure 2 shows a comparison between the neuromorphic sensor (Figures 2a and 2b) and selected frames of the Phantom high-speed camera operating at 34,000 FPS (Figure 2c). Figure 2a shows the number of cumulative On events in each pixel. The peak values of just 8 On events emphasize how dim sprites can turn out to be. Meanwhile, Figure 2b shows an attempt to illustrate time dynamics by illuminating pixels based on the timestamp associated with their first On event. In the majority of cases we explored, the earliest On events corresponded with the brightest features within sprites, and no clear time dynamics were discernible. Additionally, in most cases such as in Figure 2b, large swaths of pixels reported the exact same timestamp (to the μs), leading to portions of the sprite rendering with the exact same color. This was true in all but one captured event, which is examined in more detail during the discussion of Figure 3. Figure 2c showcases selected frames from the Phantom camera. The expected time dynamics of a sprite can be clearly seen within these screenshots. Initially, bright streamers appear in the frame, propagate downward, and rapidly branch (frames 1–3). This is followed by a uniform and gradual decay in luminosity (frames 4–6).

Of the nine analyzed sprites, we found one particularly bright case in which time dynamics was partially observable. Figure 3 showcases this event with the region in question circled. The figure has the same format as the preceding one, that is, in Figures 3a and 3b the event stream data is processed to indicate brightness and time dynamics, respectively. The highlighted feature in Figure 3 (with a red oval) shows two intersecting columns. As expected the point at which they intersect appears brightest to the sensor (Figure 3a). At the same time, the streamer tip to the right has weaker luminosity near its bottom end. Contrastingly, Figure 3b shows that the rightmost streamer is in a lighter color tone, that is, it took place earlier than the one to its left, according to the associated colorbar. Once again, this is one of the few occurrences in our data set where the apparent temporal dynamics is independent of brightness.

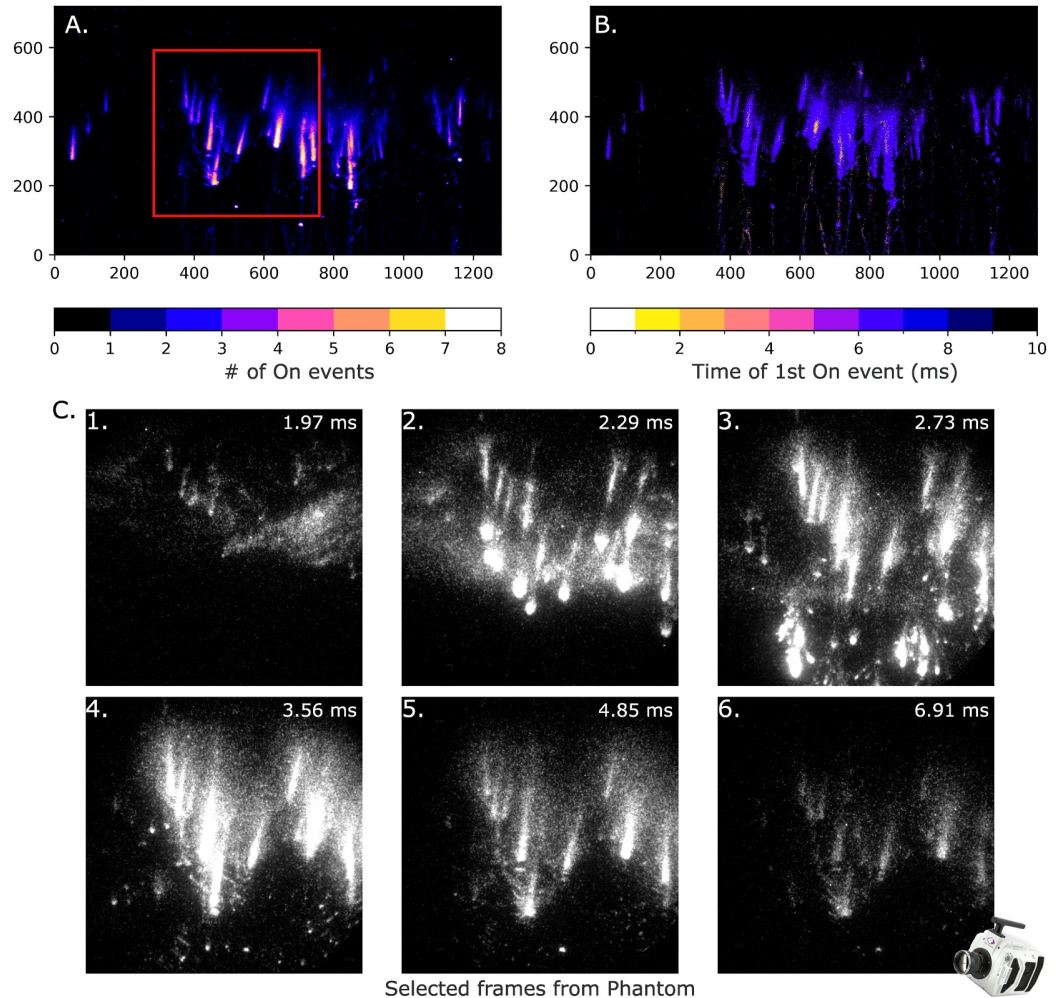


Figure 2. Sprite observed on 25 May 2023 6:53:57 UTC: comparison between neuromorphic sensor (a and b) and Phantom high-speed camera (c). (a) Integrated brightness of neuromorphic sensor. The square indicates the Phantom camera field of view. (b) Data is color-coded to indicate the time that a pixel first lights up. (c) Selected screenshots from Phantom high-speed video.

This attempt at pushing the time resolution as high as possible shows promise. However, the time dynamics of streamer motion is right at the limits of neuromorphic sensors. As discussed by McReynolds et al. (2023) and Hu et al. (2021), in low-light conditions the effective temporal resolution of a neuromorphic sensor may not surpass 1 ms. Time resolution may even be worse for very dim sources (such as sprites, see below) because of the direct relationship between light intensity incident upon the photoreceptor and the effective response time (bandwidth). In agreement with the previously-stated theory, we have found better temporal resolution and agreement with the Phantom camera in brighter sprites. Even in such cases, our maximum time resolution remains between 4 and 8 ms. In other words, we need to accumulate On events for at least 4 ms in order to construct a coherent frame. By creating bins of 4–8 ms and counting the number of On events within each period we were able to construct light curves. These light curves were then compared to light curves made by integrating the brightness of each frame captured by the Phantom camera. Figures 4a and 4b show the normalized light curves for the two sprites analyzed in this paper, (previously) reported in Figures 2 and 3, respectively. Vertical lines in Figure 4a indicate selected frames shown Figure 2c. Figures 4a and 4b show that the light curves obtained with the two different sensors agree quite well. Please note that the waveshape of these light curves should correlate very well with the electrical current flowing within sprites, as previously demonstrated (Contreras-Vidal et al., 2021; Cummer & Stanley, 1999; Cummer et al., 1998; Hager et al., 2012). Attempts of histogramming the neuromorphic sensor data in

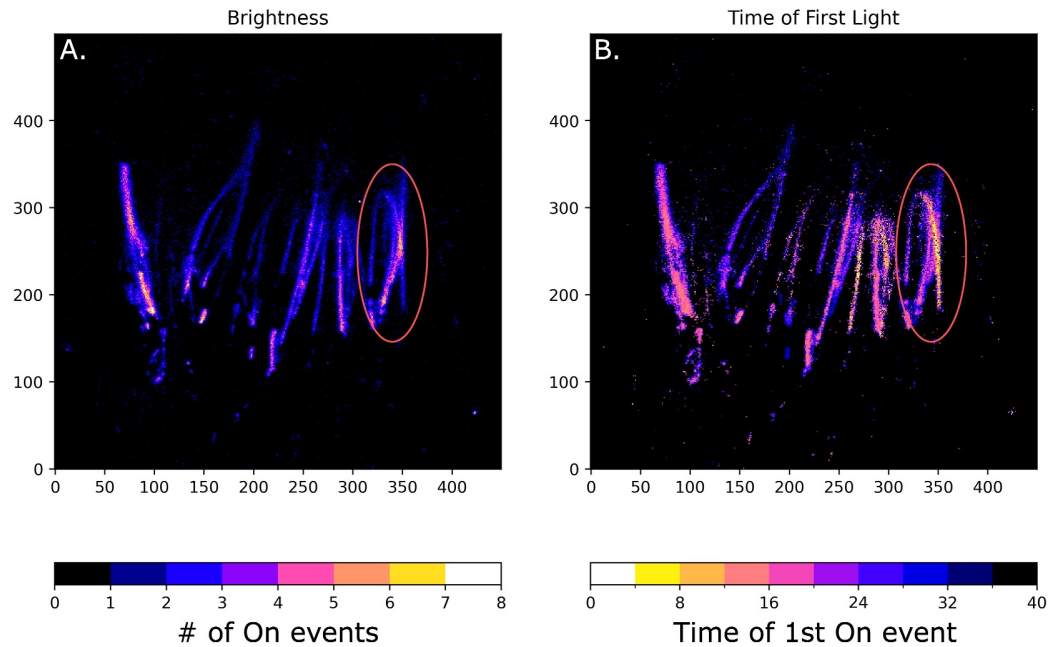


Figure 3. Sprite observed on 26 May 2023 5:26:47 UTC: a longer-duration sprite which displays some evidence of time evolution. Similarly to Figure 2, the neuromorphic sensor data is processed to display brightness (a) and onset time (b). A movie animation of this sprite has been provided as a Supporting Information S1.

shorter time windows (e.g., 1 ms) resulted in a sawtooth pattern, with events arriving in bunches every 3–4 ms (not shown). This indicates that the dead time of the sensor, under these particular observational conditions and resulting from the imposed biases settings, is 3–4 ms.

We define sprite durations as the interval between the two instants when the signal first and last exceeds 10% of the peak value in the light curve. Durations were derived for the 9 sprites detected on 25 May 2023, and a comparison between the results obtained with the two cameras can be found in Figures 4c and 4d. It can be seen that measurements for six out of the nine sprites are in reasonable-to-excellent agreement with each other (Figure 4d). In our analysis we chose to take the Phantom camera observations as the ground truth data. However, in the three cases in which the duration estimates disagree we found that some sprite activity lies outside of the (narrower) Phantom FOV. As demonstrated in Figure 4c, the discrepancy in duration estimate between the two cameras decreases with sprite brightness, providing further evidence of the relationship between sensor speed and light intensity. Across the nine sprites, the average sprite duration with the neuromorphic sensor was measured to be 55 ms with an average uncertainty of 6 ms. The average value is consistent with previous work available in the peer-reviewed literature (Bór, 2013; Hardman et al., 2000; Montanyà et al., 2010). These durations were also consistent with the Watec camera which, at 30 FPS, captured 1–3 frames per sprite.

Figure 4c indicates an inverse relationship between sprite duration and brightness. This finding begs a different interpretation of Equation 1. If we assume that the intensity of visible light emitted by the sprite is proportional to the electrical power dissipated in the mesosphere, the former can be estimated as $\text{intensity} \propto \text{available energy} / \text{duration}$. Thus, if the electrical energy available to produce sprites in the mesosphere does not vary substantially across events, intensity and duration can be expected to be inversely proportional.

4. Summary and Conclusions

Neuromorphic or event-based sensors have a lot of promise for sprite and lightning observations. This is due to two factors. First, they are inherently-fast sensors, and thus are a low-cost alternative to high-speed cameras for probing fast, transient processes within lightning and sprites. Second, they output data at a low rate, making them ideal for long duration observations, such as done from the ground by the remotely-operated LEONA network in

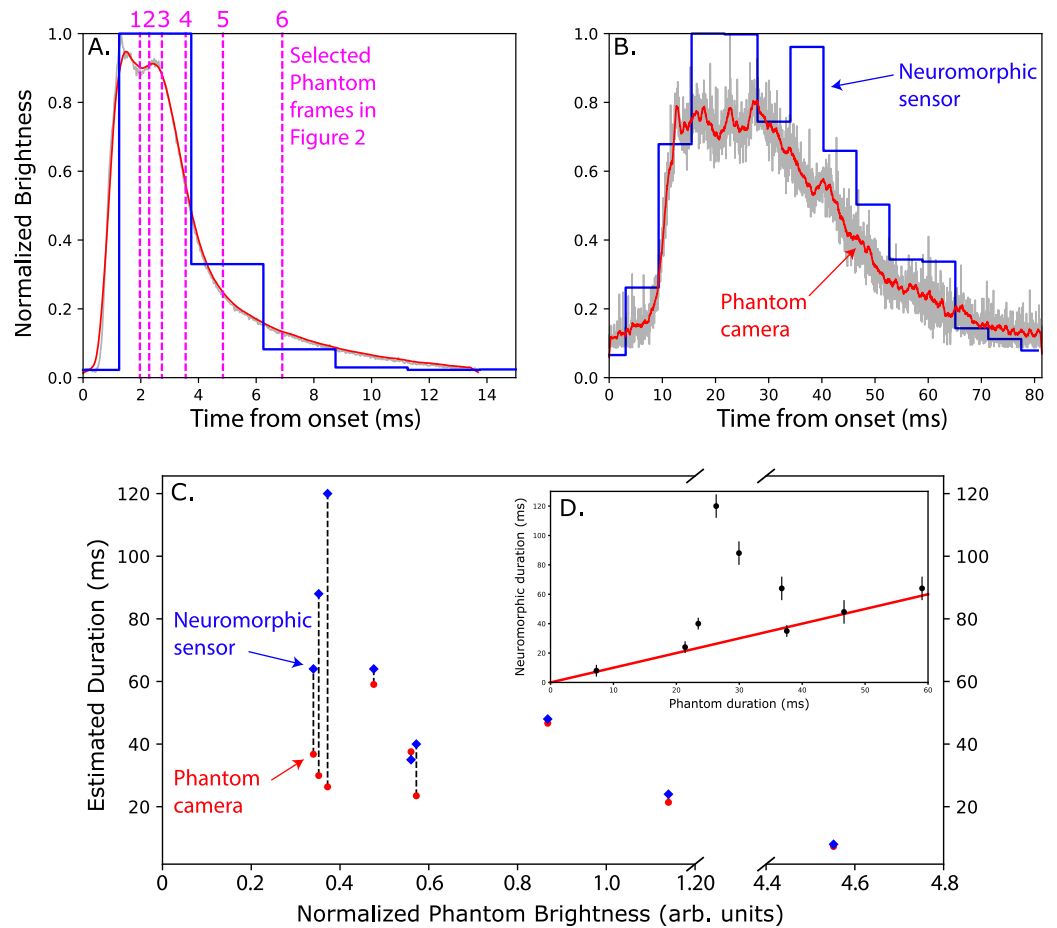


Figure 4. Analysis of durations derived from neuromorphic and Phantom cameras. (a and b) Normalized light curves illustrating brightness versus time from two separate events, which took place on 6:53:57 (a) and 5:26:47 UTC (b). (c) Sprite duration plotted versus peak sprite brightness. The latter is defined as integrated brightness across all pixels in the brightest frame of the Phantom camera, and is given in panel (c) in relative units normalized to the average across the data set. Phantom and neuromorphic data plotted in red and blue, respectively. Dashed lines connect measurements corresponding to the same event. (d) Comparison of sprite durations inferred from both cameras. The red curve ($y = x$) corresponds to a perfect agreement between the two sensors. The error bars are the bin widths used to construct the neuromorphic sensor light curves. In panel (d) the R^2 value varies between 0.09 and 0.9 with and without the inclusion of the three most significant outliers.

South America (São Sabbas et al., 2017), or in space-based missions, such as the Falcon-NEURO, Falcon-ODIN, and THOR-DAVIS onboard the ISS (Balthazor et al., 2023; Chanrion et al., 2023; McHarg et al., 2022).

In this article, we have compared a neuromorphic sensor to conventional frame based cameras for sprite observations and have determined that: (a) neuromorphic sensors can be accurately used to determine the optical lifetimes of sprites, and (b) that these sensors struggle to determine the spatiotemporal dynamics of such a dim source. The first finding has great potential toward quantifying the effects of sprites in the mesosphere, since Contreras-Vidal et al. (2021) demonstrated that sprites' optical characteristics correlate directly with their currents and, therefore, Joule heating deposition, in the mesosphere (see their Figures 1 and 9). The second finding has the caveat that the neuromorphic sensor was operated without an intensifier. Therefore, the comparison with the intensified Phantom camera is not strictly fair. In the past two decades, the vast majority of high-speed sprite observations have been aided by Phosphor intensifiers. We anticipate that their use will improve the temporal resolution of neuromorphic cameras. We shall test this hypothesis in a follow-up study.

We conclude by speculating that the use of neuromorphic sensors in atmospheric sciences will grow substantially in the coming years. Particularly, the built-in capabilities of collecting and storing data in an effective manner,

leading to low data rates, should find many uses in autonomous optical instruments, such as employed for monitoring the aurora, atmospheric gravity waves, and bolide/fireball detection.

Data Availability Statement

Data used in this article has been made publicly available online (Smith et al., 2024).

Acknowledgments

The work done by New Mexico Tech has been supported by NSF Grants AGS-1917069 and AGS-2046043 (CAREER). The work done by USAFA has been supported by the US Air Force Office of Scientific Research.

References

- Armstrong, R. A., Suszcynsky, D. M., Lyons, W. A., & Nelson, T. E. (2000). Multi-color photometric measurements of ionization and energies in sprites. *Geophysical Research Letters*, 27(5), 653–656. <https://doi.org/10.1029/1999GL003672>
- Balthazor, R. L., Wilcox, Z., George, N., McHarg, M. G., Jones, I., & Cohen, G. (2023). Event based sensor global detection of lightning from the International Space Station compared with traditional lightning detection networks. In *Paper presented at the 2023 American Geophysical Union (AGU) Fall Meeting*. (Abstract AE33B-07).
- Bocippio, D. J., Williams, E. R., Heckman, S. J., Lyons, W. A., Baker, I. T., & Boldi, R. (1995). Sprites, ELF transients, and positive ground strokes. *Science*, 269(5227), 1088–1091. <https://doi.org/10.1126/science.269.5227.1088>
- Bór, J. (2013). Optically perceptible characteristics of sprites observed in Central Europe in 2007–2009. *Journal of Atmospheric and Solar-Terrestrial Physics*, 92, 151–177. <https://doi.org/10.1016/j.jastp.2012.10.008>
- Brandli, C., Muller, L., & Delbruck, T. (2014). Real-time, high-speed video decompression using a frame- and event-based DAVIS sensor. In *Paper presented at 2014 IEEE International Symposium on Circuits and Systems (ISCAS)* (pp. 686–689). <https://doi.org/10.1109/ISCAS.2014.6865228>
- Chanrion, O., Pedersen, N., Yair, Y., Stendel, M., Li, D., Stokholm, A., & Neubert, T. (2023). THOR-DAVIS: A neuromorphic camera for thunderstorm observation from the International Space Station (ISS). In *Paper presented at the 2023 American Geophysical Union (AGU) Fall Meeting*. (Abstract AE01A-08).
- Contreras-Vidal, L., Sonnenfeld, R. G., da Silva, C. L., McHarg, M. G., Jensen, D., Harley, J., et al. (2021). Relationship between sprite current and morphology. *Journal of Geophysical Research: Space Physics*, 126(3), e2020JA028930. <https://doi.org/10.1029/2020JA028930>
- Cummer, S. A., Inan, U. S., Bell, T. F., & Barrington-Leigh, C. P. (1998). ELF radiation produced by electrical currents in sprites. *Geophysical Research Letters*, 25(8), 1281–1284. <https://doi.org/10.1029/98GL50937>
- Cummer, S. A., & Stanley, M. (1999). Submillisecond resolution lightning currents and sprite development: Observations and implications. *Geophysical Research Letters*, 26(20), 3205–3208. <https://doi.org/10.1029/1999GL003635>
- da Silva, C. L., & Pasko, V. P. (2014). Infrasonic acoustic waves generated by fast air heating in sprite cores. *Geophysical Research Letters*, 41(5), 1789–1795. <https://doi.org/10.1002/2013GL059164>
- da Silva, C. L., & São Sabbas, F. T. (2013). Consequences of the application of the streamer fluid model to the study of the sprite inception mechanism. *Advances in Space Research*, 51(10), 1902–1915. <https://doi.org/10.1016/j.asr.2012.11.025>
- Fraknoi, A., Morrison, D., & Wolff, S. C. (2018). Astronomy 2e. Retrieved from <https://openstax.org/details/books/astronomy-2e>
- Gordillo-Vazquez, F. J. (2008). Air plasma kinetics under the influence of sprites. *Journal of Physics D: Applied Physics*, 41(23), 234016. <https://doi.org/10.1088/0022-3727/41/23/234016>
- Hager, W. W., Sonnenfeld, R. G., Feng, W., Kanmae, T., Stenbaek-Nielsen, H. C., McHarg, M. G., et al. (2012). Charge rearrangement by sprites over a north Texas mesoscale convective system. *Journal of Geophysical Research*, 117(D22), D22101. <https://doi.org/10.1029/2012JD018309>
- Hardman, S. F., Dowden, R. L., Brundell, J. B., Bahr, J. L., Kawasaki, Z.-i., & Rodger, C. J. (2000). Sprite observations in the Northern Territory of Australia. *Journal of Geophysical Research*, 105(D4), 4689–4697. <https://doi.org/10.1029/1999JD900325>
- Holesovsky, O., Skoviera, R., Hlavac, V., & Vitek, R. (2021). Experimental comparison between event and global shutter cameras. *Sensors*, 21(4), 1137. <https://doi.org/10.3390/s21041137>
- Hu, Y., Liu, S.-C., & Delbruck, T. (2021). v2e: From video frames to realistic DVS events. In *Proceedings of the IEEE/CVF Conference on Computer Vision and Pattern Recognition (CVPR) Workshops* (pp. 1312–1321).
- Kanmae, T., Stenbaek-Nielsen, H. C., & McHarg, M. G. (2007). Altitude resolved sprite spectra with 3 ms temporal resolution. *Geophysical Research Letters*, 34(7), L07810. <https://doi.org/10.1029/2006GL028608>
- Kanmae, T., Stenbaek-Nielsen, H. C., McHarg, M. G., & Haaland, R. K. (2012). Diameter-speed relation of sprite streamers. *Journal of Physics D: Applied Physics*, 45(27), 275203. <https://doi.org/10.1088/0022-3727/45/27/275203>
- Luque, A., & Ebert, U. (2009). Emergence of sprite streamers from screening-ionization waves in the lower ionosphere. *Nature Geoscience*, 2(11), 757–760. <https://doi.org/10.1038/ngeo662>
- McHarg, M. G., Balthazor, R. L., McReynolds, B. J., Howe, D. H., Maloney, C. J., O’Keefe, D., et al. (2022). Falcon Neuro: An event-based sensor on the International Space Station. *Optical Engineering*, 61(8), 085105. <https://doi.org/10.1117/1.OE.61.8.085105>
- McHarg, M. G., Haaland, R. K., Moudry, D., & Stenbaek-Nielsen, H. C. (2002). Altitude-time development of sprites. *Journal of Geophysical Research*, 107(A11), SIA 9-1–SIA 9-12. <https://doi.org/10.1029/2001JA000283>
- McReynolds, B. J., Graca, R., O’Keefe, D., Oliver, R., Balthazor, R., George, N., & McHarg, M. (2023). Modeling and decoding event-based sensor lightning response. In J. J. Dolne, M. F. Spencer, & S. R. Bose-Pillai (Eds.), *Unconventional imaging, sensing, and adaptive optics 2023* (Vol. 12693, p. 1269313). SPIE. <https://doi.org/10.1117/12.2674435>
- Montanya, J., van der Velde, O., Romero, D., March, V., Solà, G., Pineda, N., et al. (2010). High-speed intensified video recordings of sprites and elves over the western Mediterranean Sea during winter thunderstorms. *Journal of Geophysical Research*, 115(A4), A00E18. <https://doi.org/10.1029/2009JA014508>
- Pasko, V. P. (2010). Recent advances in theory of transient luminous events. *Journal of Geophysical Research*, 115(A6), A00E35. <https://doi.org/10.1029/2009JA014860>
- Pasko, V. P., Inan, U. S., Bell, T. F., & Taranenko, Y. N. (1997). Sprites produced by quasi-electrostatic heating and ionization in the lower ionosphere. *Journal of Geophysical Research*, 102(A3), 4529–4561. <https://doi.org/10.1029/96JA03528>
- Qin, J., Celestin, S., & Pasko, V. P. (2012). Formation of single and double-headed streamers in sprite-halo events. *Geophysical Research Letters*, 39(5), L05810. <https://doi.org/10.1029/2012GL051088>
- Qin, J., Celestin, S., Pasko, V. P., Cummer, S. A., McHarg, M. G., & Stenbaek-Nielsen, H. C. (2013). Mechanism of column and carrot sprites derived from optical and radio observations. *Geophysical Research Letters*, 40(17), 4777–4782. <https://doi.org/10.1002/GRL.50910>

- Qin, J., Pasko, V. P., McHarg, M. G., & Stenbaek-Nielsen, H. C. (2014). Plasma irregularities in the D-region ionosphere in association with sprite streamer initiation. *Nature Communications*, 5(1), 3740. <https://doi.org/10.1038/ncomms4740>
- Rairden, R. L., & Mende, S. B. (1995). Time resolved sprite imagery. *Geophysical Research Letters*, 22(24), 3465–3468. <https://doi.org/10.1029/95GL03332>
- São Sabbas, F., Souza, J. R. D., Guerra, E. M., Filho, A. C. J., Galvão, R. M. O., Branco, R., et al. (2017). LEONA for TLE and HEET research in South America. In *Paper presented at the 2017 American Geophysical Union (AGU) Fall Meeting*. (Abstract AE21A-05).
- Scheerlinck, C. (2021). How to see with an event camera. PQDT - Global, 132.
- Sentman, D. D., & Stenbaek-Nielsen, H. C. (2009). Chemical effects of weak electric fields in the trailing columns of sprite streamers. *Plasma Sources Science and Technology*, 18(3), 034012. <https://doi.org/10.1088/0963-0252/18/3/034012>
- Sentman, D. D., Stenbaek-Nielsen, H. C., McHarg, M. G., & Morrill, J. S. (2008). Plasma chemistry of sprite streamers. *Journal of Geophysical Research*, 113(D11), D11112. <https://doi.org/10.1029/2007JD008941>
- Sentman, D. D., Wescott, E., Picard, R., Winick, J., Stenbaek-Nielsen, H., Dewan, E., et al. (2003). Simultaneous observations of mesospheric gravity waves and sprites generated by a midwestern thunderstorm. *Journal of Atmospheric and Solar-Terrestrial Physics*, 65(5), 537–550. [https://doi.org/10.1016/S1364-6826\(02\)00328-0](https://doi.org/10.1016/S1364-6826(02)00328-0)
- Smith, B., McHarg, M. G., da Silva, C. L., Sonnenfeld, R. G., Koile, J., Leal, A. F. R., & Jones, I. R. (2024). Sprite observations made from Langmuir Lab with a neuromorphic sensor on May 25, 2023 [Dataset]. *Zenodo*. <https://doi.org/10.5281/zenodo.10835753>
- Stenbaek-Nielsen, H. C., Haaland, R., McHarg, M. G., Hensley, B. A., & Kanmae, T. (2010). Sprite initiation altitude measured by triangulation. *Journal of Geophysical Research*, 115(A3), A00E12. <https://doi.org/10.1029/2009JA014543>
- Stenbaek-Nielsen, H. C., Kanmae, T., McHarg, M. G., & Haaland, R. (2013). High-speed observations of sprite streamers. *Surveys in Geophysics*, 34(6), 769–795. <https://doi.org/10.1007/s10712-013-9224-4>
- Stenbaek-Nielsen, H. C., McHarg, M. G., Kammae, T., & Sentman, D. D. (2007). Observed emission rates in sprite streamer heads. *Geophysical Research Letters*, 34(11), L11105. <https://doi.org/10.1029/2007GL029881>
- Winckler, J. R., Lyons, W. A., Nelson, T. E., & Nenzek, R. J. (1996). New high-resolution ground-based studies of sprites. *Journal of Geophysical Research*, 101(D3), 6997–7004. <https://doi.org/10.1029/95JD03443>